

THERMAL NOISE ANALYSIS OF THE RESISTIVE VEE DIPOLE

S. Park

DMC R&D Center
Samsung Electronics Corporation
Suwon, Republic of Korea

K. Kim

School of Information and Mechatronics
Gwangju Institute of Science and Technology
Gwangju, Republic of Korea

Abstract—The thermal noise of the resistive vee dipole (RVD) has been analyzed using a numerical model based on the method of moments. The RVD analyzed in this paper has curved arms and is loaded with surface-mount chip resistors, which approximate a modified Wu-King profile. The total noise power delivered to a 200 Ω feed line and the contribution of individual resistors to the total noise power are presented. The results show that the noise temperature of the RVD is very high and the resistors close to the drive point contribute more to the total noise power than do the resistors close to the open ends of the antenna arms.

1. INTRODUCTION

The resistive vee dipole (RVD) is a vee antenna, whose arms are loaded resistively according to a loading profile [1, 2]. In many applications, the Wu-King profile is selected for the loading profile, which can be expressed as the resistance per unit length [3–6]

$$R(z) = \frac{R_0}{1 - z/L}, \quad 0 \leq z \leq L, \quad (1)$$

where z is the distance measured along the arm from the drive point, L is the length of the arm, and R_0 is the resistance per unit length at the

Corresponding author: K. Kim (mkkim@gist.ac.kr).

drive point. With the Wu-King profile, the resistance per unit length of the antenna arms increases to an infinite value at the open ends of the antenna arms. The Wu-King profile suppresses the internal reflection of the current in the antenna arms. Thus, when a pulse is applied in the feed line, the RVD with the Wu-King profile produces essentially no ripples in the feed line except for the initial reflection at the drive point. The RVD can also send and receive short pulses in a directional fashion and has a low radar cross section, which can minimize multiple reflections between the antenna and nearby objects. In addition, the RVD can easily be applied in array applications. These features of the RVD make it suitable for many ground-penetrating radar (GPR) applications [7–12].

However, the GPR with the RVD may have a limited sounding depth. The sounding depth may be affected by many factors. One factor is the limited power handling capability of the loading resistors, which limits the amount of power that can be accepted from the feed line. For example, the amount of power that can be accepted by the RVD with chip resistor loading is limited by the power handling capability of the chip resistors. At most frequencies, the first resistor from the drive point dissipates more power than the other resistors, though the first resistor has the lowest resistor value [13]. Thus, the power rating of the first resistor determines the maximum power that can be accepted by the RVD, which in turn determines the maximum power that can be transmitted.

Another factor limiting the sounding depth is the amount of noise power. When the RVD is in the receiving mode, the received signal may be amplified to a useful level if the signal power is stronger than the noise power. If the signal power is limited, the amount of noise power limits the sounding depth. Thus, the purpose of this paper is to investigate the noise behavior of the RVD at the drive point of the antenna. In this paper, only the thermal noise from the resistive loading is considered because the thermal noise is inherent in the antenna and cannot be avoided. A numerical model based on a commercial method of moments software is used for the investigation.

2. NUMERICAL MODEL

The geometry of the antenna analyzed in this paper is the RVD with a curved shape and a modified Wu-King profile, which was presented in [14]. The profile can be expressed as

$$R_m^{-1}(z) = \frac{1 - z/L}{R_0} + \frac{(1 - z/L)^2}{R_1}, \quad 0 \leq z \leq L, \quad (2)$$

where R_1 is the modification parameter. The profile is equivalent to Equation (1) when $R_1 \rightarrow \infty$. Here, $R_0L = R_1L = 467.1 \Omega$ is selected. The modified Wu-King profile, which is continuous, is approximated with 14 chip resistors loaded on each arm. The values of the resistors are shown in Table 1. Note that the resistor values in Table 1 are available off-the-shelf. Table 1 shows that the resistor value is the smallest near the drive point and gradually increases toward the open ends of the antenna arms.

The geometry is discretized for the method of moments calculation. The arms and the resistors are meshed using triangular elements. The copper portion is modeled as a perfect electric conductor (PEC) and the resistors are modeled using resistive sheets. Figure 1 shows the mesh for the numerical model. The software used for the mesh generation and calculation is FEKO, which is a collection of frequency domain algorithms [15]. In this paper, only the method of moments is used.

The resistive sheets are much smaller than the wavelength of interest in this paper and thus can be considered as lumped resistors. The mean square noise voltage per hertz of bandwidth generated by a lumped resistor is [16]

$$v_n^2 = 4kTR, \tag{3}$$

Table 1. Resistor values in Ohms for the antenna loading.

R_1	R_2	R_3	R_4	R_5	R_6	R_7
17.8	19.6	22.1	25.5	29.4	34.0	40.2
R_8	R_9	R_{10}	R_{11}	R_{12}	R_{13}	R_{14}
49.9	60.4	78.7	107	158	280	887

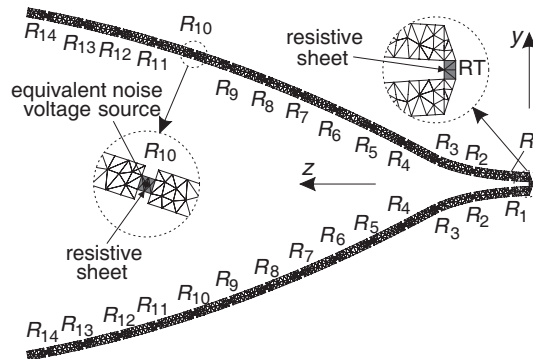


Figure 1. Mesh for the numerical model of the resistive vee dipole.

where k is the Boltzmann's constant; $T = 300\text{ K}$ is the physical temperature; R is the resistance. The noise voltage can be modeled with a power-equivalent sinusoidal voltage source

$$v_{eq}(t) = \sqrt{2}\sqrt{4kTR}\cos(2\pi ft), \quad (4)$$

where f and t are the frequency and time, respectively. The equivalent source is placed in the middle of each resistive sheet. To simulate the feed line impedance, a terminal resistor (RT) of $200\ \Omega$ is placed between the terminals at the drive point.

The contribution of a resistor to the noise power accepted by the feed line is obtained by activating the corresponding equivalent source and calculating the power absorbed by the terminal resistor. The total noise power accepted by the feed line is obtained by summing the contributions of the individual resistors, i.e.,

$$P_n = 2 \sum_{i=1}^N P_{n,i}, \quad (5)$$

where $P_{n,i}$ is the noise power contribution of the i -th resistor, and $N = 14$ is the total number of resistors on one arm. The factor 2 is present because of the symmetry in the antenna geometry. Thus, for the total noise power calculation, the model is run 14 times for the 14 resistor values, activating one equivalent source at a time at each frequency of interest.

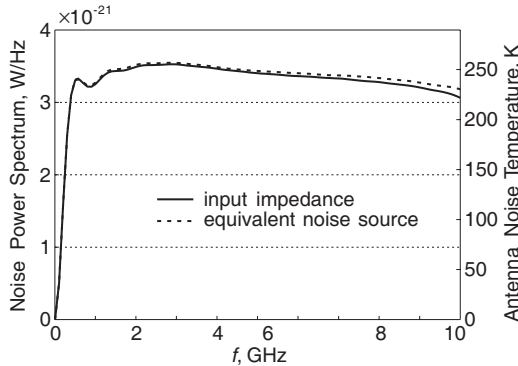


Figure 2. Spectrum of noise power delivered to the $200\ \Omega$ feed line and corresponding antenna noise temperature for $T = 300\text{ K}$. Solid line: calculated using input impedance and efficiency of the antenna. Dashed line: calculated using equivalent noise sources and a $200\ \Omega$ resistor simulating the feed line impedance.

The total noise power calculated using the equivalent noise source is drawn in a dashed line against frequency in Figure 2. The dashed line represents the total noise power that is delivered to the feed line of the RVD. In the figure, the vertical axis on the left-hand side represents the noise power spectrum, which is the noise power per hertz of bandwidth.

In order to validate the result, the thermal noise power is calculated in a different way. The thermal noise power accepted by the feed line of an antenna can be calculated as [17, 18]

$$P_n = kTB(1 - \eta)(1 - |\Gamma|^2), \quad (6)$$

where B is the receiver bandwidth; η is the radiation efficiency of the antenna; Γ is the reflection coefficient between the antenna and the feed line. Thus, the noise power can also be calculated from the input impedance and the radiation efficiency of the antenna. These quantities can be calculated by slightly modifying the numerical model. The terminal resistor is removed, and a voltage source is placed between the terminals to excite the antenna. All other equivalent sources are turned off. This model is run once for the calculation of the input impedance and the antenna radiation efficiency. The efficiency is read directly from the FEKO output file and the antenna input impedance is converted to the reflection mismatch using

$$\Gamma = \frac{Z_{in} - Z_0}{Z_{in} + Z_0}, \quad (7)$$

where Z_{in} is the antenna input impedance, and $Z_0 = 200 \Omega$ is the feed line impedance. The solid line in Figure 2 represents the thermal noise power obtained from Equation (6).

The two lines in Figure 2 are very close to each other, validating the equivalent noise source approach. The small difference seen at the high frequency region is due to numerical error, which can be lowered by using a finer mesh. The figure shows that the equivalent noise voltage can be used for further analysis with only a small error. The maximum error is 3.84% at the highest frequency.

3. THERMAL NOISE ANALYSIS

The vertical axis on the right hand side of Figure 2 represents the antenna noise temperature corresponding to the noise power spectrum. The noise temperature is very high compared to those of other conventional antennas. For example, the noise temperature of a dipole antenna with the wire radius of $3 \times 10^{-3} \lambda$ is approximately 1.2 K when driven by a 50Ω feed line at resonant frequency. As an example of the antenna with a low radiation efficiency, a commercial chip

antenna with a radiation efficiency of 75% has the noise temperature of approximately 67 K [19].

As can be seen in Equation (3), the higher the resistor value is, the higher the thermal noise voltage. However, the resistors with higher resistances are located farther from the drive point of the RVD, and the noise power generated from these resistors may not reach the antenna terminals efficiently. Thus, the resistor value and the amount of noise power delivered to the antenna terminals may not be directly related.

In order to investigate how much noise power is contributed from each resistor, the noise power contribution is plotted against resistor number at a number of frequencies in Figure 3. The figure shows the contribution of individual resistors to the total noise power delivered to the $200\ \Omega$ feed line. The arrows in the figure indicate the change in noise contribution as the frequency varies from 2.0 GHz to 10 GHz with 0.5 GHz increment. Those at 0.5, 1.0, and 1.5 GHz are drawn in dot, dash-dot, and dash-dot-dot lines, respectively. Note that there are two resistors in the RVD for each resistor number. Thus, the lines in Figure 3 represents the contributions from the resistor on one arm, and the summation of the noise contribution at each frequency is 50%.

Figure 3 shows the tendency that resistors close to the drive point contribute more to the noise power than do the resistors far from the drive point even though the latter have higher resistance. This tendency becomes stronger as the frequency increases. This figure suggests that the noise temperature of the antenna can be decreased significantly by lowering the noise contributions from a few resistors near the drive point.

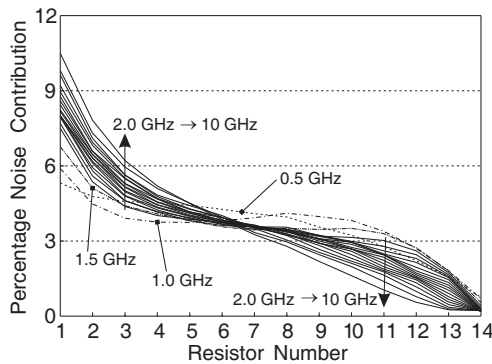


Figure 3. Contribution of individual resistors to the noise power delivered to the $200\ \Omega$ feed line. The arrows indicate the change in noise contribution as the frequency varies from 2.0 GHz to 10 GHz with 0.5 GHz increment.

4. CONCLUSION

The noise characteristics of the RVD were numerically analyzed using the method of moments and equivalent noise voltage sources. The RVD analyzed in this paper has curved arms and is loaded with the modified Wu-King profile. The total thermal noise power delivered to the $200\ \Omega$ feed line and the contribution of individual resistors to the total noise power were presented. The results showed that the antenna noise temperature is very high and that the resistors near the drive point contribute more to the noise temperature. Because the high noise temperature limits the reception capability of the RVD, the operational range of the radar with the RVD would be limited accordingly. The results shown in this paper may be used to determine the operation range of the RVD as antennas for radars, such as ground-based GPR, airborne GPR, and vehicle-mounted foliage-penetration radar.

ACKNOWLEDGMENT

This work was supported in part by UTRC programs supported by Agency for Defense Development and in part by Defense Acquisition Program Administration and Agency for Defense Development under the contract UD070017AD.

REFERENCES

1. Montoya, T. P. and G. S. Smith, "Resistively-loaded vee antennas for short-pulse ground penetrating radar," *IEEE Int. Antennas Propagat. Symp. Dig.*, 2068–2071, 1996.
2. Kim, K., "Numerical and experimental investigation of impulse-radiating antennas for use in sensing applications," Ph.D. dissertation, Georgia Institute of Science and Technology, 2003.
3. Wu, T. T. and R. W. P. King, "The cylindrical antenna with nonreflecting resistive loading," *IEEE Trans. Antennas Propagat.*, Vol. 13, No. 3, 369–373, 1965.
4. Shen, L. C. and R. W. P. King, "Correction to 'The cylindrical antenna with nonreflecting resistive loading'," *IEEE Trans. Antennas Propagat.*, Vol. 13, No. 6, 998, 1965.
5. Maloney, J. G. and G. S. Smith, "A study of transient radiation from the Wu-King resistive monopole — FDTD analysis and experimental measurements," *IEEE Trans. Antennas Propagat.*, Vol. 41, No. 5, 668–676, 1993.

6. Maloney, J. G. and G. S. Smith, "Correction to 'A study of transient radiation from the Wu-King resistive monopole — FDTD analysis and experimental measurements'," *IEEE Trans. Antennas Propagat.*, Vol. 43, No. 2, 226, 1995.
7. Counts, T., A. C. Gurbuz, W. R. Scott, J. H. McClellan, and K. Kim, "Multistatic ground-penetrating radar experiments," *IEEE Trans. Antennas Propagat.*, Vol. 45, No. 8, 2544–2553, 2007.
8. Montoya, T. P. and G. S. Smith, "Vee dipoles with resistive loading for short-pulse ground-penetrating radar," *Microw. Opt. Tech. Lett.*, Vol. 13, No. 3, 132–137, 1996.
9. Montoya, T. P. and G. S. Smith, "Land mine detection using a ground-penetrating radar based on resistively loaded vee dipoles," *IEEE Trans. Antennas Propagat.*, Vol. 47, No. 12, 1795–1806, 1999.
10. Scott, W. R., K. Kim, G. D. Larson, A. C. Gurbuz, and J. H. McClellan, "Combined seismic, radar, and induction sensor for landmine detection," *Proc. IEEE Int. Geosci. Remote Sensing Symp.*, 1613–1616, 2004.
11. Scott, W. R., K. Kim, and G. D. Larson, "Investigation of a combined seismic, radar, and induction sensor for landmine detection," *J. Acoust. Soc. Am.*, Vol. 15, No. 5, 2415, 2004.
12. Guo, Y. C., L. Xu, and X. W. Shi, "Improved loading profile for GPR antenna applications," *Journal of Electromagnetic Waves and Applications*, Vol. 21, No. 10, 1367–1378, 2007.
13. Kim, K. and S. Yang, "Efficiency of resistive vee dipole antenna," *Electron. Lett.*, Vol. 43, No. 22, 1169–1171, 2007.
14. Kim, K. and W. R. Scott, "Design of a resistively-loaded vee dipole for ultra-wideband ground-penetrating radar applications," *IEEE Trans. Antennas Propagat.*, Vol. 53, No. 8, 2525–2532, 2005.
15. FEKO Website, available online: <http://www.feko.info>.
16. Kittel, C., *Elementary Statistical Physics*, Wiley, New York, 1958.
17. Craeye, C., "Including spatial correlation of thermal noise in the noise model of high-sensitivity arrays," *IEEE Trans. Antennas Propagat.*, Vol. 53, No. 11, 3845–3848, 2005.
18. Collin, R. E. and F. J. Zucker, *Antenna Theory, Part I*, McGraw-Hill, New York, 1969.
19. "Rufa 2.4 GHz SMD Antenna," available online: <http://www.antenna.com>.